

**Research Article**
**Open Access**

## Assessing the Accuracy of LiDAR Surveys for Geodetic Mass Balances in Glaciers of Chilean Central Andes

Gonzalo Barcaza<sup>1\*</sup>, Felipe Gómez<sup>2</sup>, Ximena Fadic<sup>1</sup>, Felipe Mccracken<sup>2</sup>, Guillermo Tapia<sup>3</sup> and Francisco Cereceda Balic<sup>1,4</sup>

<sup>1</sup>Center for Environmental Technologies, Federico Santa María Technical University (CETAM-UTFSM), Valparaíso, Chile

<sup>2</sup>Department of Civil Engineering, Federico Santa María Technical University, Valparaíso, Chile

<sup>3</sup>General Directorate of Water, Ministry of Public Works, Santiago, Chile

<sup>4</sup>Department of Chemistry, Federico Santa María Technical University (UTFSM), Valparaíso, Chile

### ABSTRACT

Repeat high-resolution (1m<sup>2</sup>) airborne light radio detection and ranging (LiDAR) laser altimetry data (2009-2015) for geodetic mass balances on five mountain glaciers, and its near-time ground-control points (GCPs) surveyed by global positioning system (GPS) on glacier surface (2015), were firstly used for accuracy assessment of elevation changes (dh/dt) in Chilean Central Andes. The inverse distance weighting algorithm (IDW) reproduced the glacier surface topography with the minimum root mean square error (RMSE) when a digital elevation model (DEM) is created. High thinning rates in meter water equivalent (mw.e.) were found at Echaurren Norte and San Francisco glaciers, two partially covered low-elevation glaciers, with  $-1.69 \pm 0.14$  m and  $-1.3 \pm 0.19$  m, respectively, while at Yeso and Bello, two high-altitude clean-ice glaciers, a more moderate rate of  $-0.65 \pm 0.24$  m and  $-0.66 \pm 0.14$  m was derived. Likewise, Pirámide is a debris-covered glacier with a negligible elevation change. Although systematic and random errors using glacierized and non-glacierized terrain shows neglected differences, inaccuracies induced by pre-processing interpolation parameters yield positive and negatives differences of up to 2.04 m which leads to 3% biases in the geodetic mass balances.

### \*Corresponding author

Gonzalo Barcaza, Center for Environmental Technologies, Federico Santa María Technical University (CETAM-UTFSM), Valparaíso, Chile.

**Received:** March 15, 2025; **Accepted:** March 18, 2025; **Published:** April 11, 2025

**Keywords:** Chilean Central Andes, Geodetic Mass Balance, LiDAR, Accuracy Assessment

### Introduction

Mountain glaciers worldwide are shrinking and thinning at unprecedented high rates during the 20<sup>th</sup> century in response to global warming, including glacier disintegration, and larger ablation rates induced by decreasing albedo on glaciers [1-6]. These changes have been estimated using the traditional glaciological mass balance method, which rely on intensive ground-based measurements (snow pits and ablation stakes) at selected benchmark glaciers, and the geodetic mass balance method which is based upon glacier surface elevation change (dH/dt) derived from ground-truth measurements such as global positioning system (GPS) or remotely sensed derived digital elevation models (DEMs) [7-11]. The comparison between both mass balance methods has been of main concern since the geodetic method enables to monitor large and high altitudes glaciers with jagged topography where ground-truth data is not possible [9,12].

In the geodetic method the glacier surface elevation (H) is compiled as elevation time series, H(t), from which inter-annual rate of change in elevation (dH/dt) is derived (ma<sup>-1</sup>) by subtracting the glacier elevation values from two time-spanning DEMs. To derive a reliable inter-annual rate of elevation change, the geodetic method requires that surface elevation data should be acquired at the end of late-summer season, and the surface density (snow and ice) is

required for assessing the mass balance in water equivalent (ma<sup>-1</sup> w.e.) [13-15]. DEMs from high-resolution satellite images requires orbital ephemerides to be computed while DEMs from airborne light radio detection and ranging (LiDAR) altimetry surveys uses inertial movement unit (IMU) together with a simultaneous GPS system (on board and ground-based) [16,17]. Despite the wide availability of higher-resolution data from satellite images or LiDAR altimetry surveys, accuracy assessment on glacier surface is still relevant to avoid pre-processing induced biases [18-20].

In the absence of ground-truth data, accuracy assessment normally involves non-glacierized rocky areas as invariant targets, data that can be exposed to same error sources during the survey. Random or stochastic errors in glacier-elevation data ( $\sigma_z$ ) is of main concern to the elevation change (dh/dt) while the glacier area delimitation ( $\sigma_A$ ) around the glacier outline also accounts for total uncertainty of the DEM [21-23]. Mass balance estimates using remote sensing in Chilean Central Andes still lack of ground-truth validation on glacier surface.

Repeat airborne LiDAR surveys available on five mountain glaciers were carried out for Dirección General de Aguas (DGA), the Chilean water agency, by two private consultancy firms, while ground control points (GCP) for accuracy assessment on glacier surface was performed by a ground-party of DGA. This unique near-time data, acquired within a month of delay in the late-summer season of 2015, combines high-resolution ( $\pm 1$ m) LiDAR

altimetry surveys, covering both glacierized and non-glacierized rocky areas, together with GCP surveyed with a geodetic-quality GPS.

DEM creation, from cloud-points to raster, first essayed four spatial data interpolation algorithms to obtain the one which better represents the glacier surface topography according to GCP values [24]. The minimum stochastic uncertainties were estimated by means of the root-mean square error (RMSE) between GCP and its interpolated pixel value. Secondly, we essayed differences in error estimates by changing pre-processing parameters within the same interpolation algorithm. Then, these parameters yielding the DEM with the minimum RMSE (hereafter DEM/2015), were applied to repeat LiDAR altimetry surveys available for 2009 (hereafter DEM/2009) and 2012 (hereafter DEM/2012) to update the geodetic mass balance up to 2015. Error analyzes also included the total uncertainty of the DEM considering both systematic and random errors by comparing both GCP and rocky areas instead as ground-truth validation.

In this paper, we investigate the accuracy of LiDAR survey for geodetic mass balance on five mountain glaciers of Central Andes using ground-truth data and pre-processing parameters for DEM creation by applying four interpolation algorithms. We aim to

- assess the accuracy of DEMs derived from LiDAR surveys using near-time GCP points surveyed at pixel scale;
- compare different geometric parameters for DEM creation;
- determine bias in mass balances values induced by DEM interpolation.

### Study Area

Ground-truth measurements for validation were performed at Yeso (ca. 2.03 km<sup>2</sup>), Bello (ca. 4.22 km<sup>2</sup>), San Francisco (ca. 1.29 km<sup>2</sup>), Echaurren Norte (ca. 0.23 km<sup>2</sup>) and Pirámide (ca. 4.40 km<sup>2</sup>) glaciers, all of them are mountain glaciers located at different small sub-catchments of Maipo catchment (Figure 1).

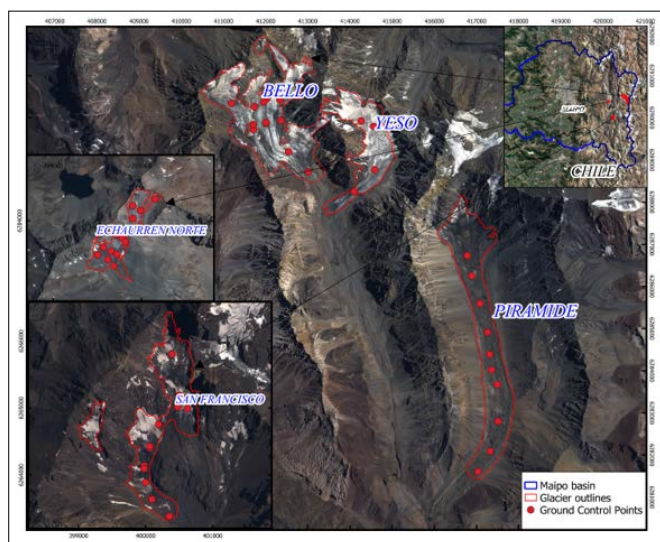


**Figure 1:** Location of Echaurren Norte, San Francisco, Pirámide, Bello and Yeso glaciers at Maipo basin and spatial distribution of 56 points surveyed with global positioning system

Central Andes (32°–36°S) extends from north to south between Aconcagua and Mataquito catchments, covering a glacierized area of about 869.5 km<sup>2</sup> [25]. Climate change is causing negative mass balances in the glaciers of the Central Andes [26,27]. A warming trend of +0.26 °C/decade (1976–2006) was determined between 17° and 37° S as well as the reduction in precipitation of 3.7%/decade (1979 - 2008) due to the extended mega-drought during the last decade [28-30].

Mass balance estimates at Central Andes had been derived using from ASTER DEMs (30 m spatial resolution) and the Shuttle Radar Topographic Mission (SRTM) at two times between 2000 and 2018. ASTER DEMs was created using the Ames Stereo Pipeline (ASP) open-source software package while the SRTM was calibrated in the vertical but ground control points were lacking [16,31]. Glacier outlines were obtained from the Randolph Glacier Inventory (RGI 6.0) and the elevation change by region was adjusted to a linear regression. A total thinning rate of  $-0.72 \pm 0.22$  m w.e. a<sup>-1</sup> was obtained, in which the estimated error by region is 32% for Patagonia, 57% for Tropical Andes and 64% for Dry Andes. Likewise, at Central Andes an increased thinning rate from  $0.13 \pm 0.05$  m w.e. a<sup>-1</sup> between 1955 and 2000 to  $-0.18 \pm 0.08$  w.e. a<sup>-1</sup> between 2000-2013 was found using a combination of former inventory data, the SRTM and LiDAR surveys.

Mass balance investigations at Echaurren Norte glacier started in 1975, which is the largest mass balance record of South America [26]. The glacier has become fully covered with debris as permanent thinning has been affecting the entire glacier area. It is the smallest glacier analyzed, and it lacks a well-defined terminus from its surrounding non-glacierized terrain. The glacier doesn't have crevassed areas, and its surface conditions are composed of bumpy topography and large boulders.

San Francisco glacier is a clean-ice glacier exposed to south-west, which has been getting fully covered with debris prior to 2009 and is affected by large land slides from its upper wall sides as well as at its lower elevations which feeds an increasingly thicker debris-coverage. The glacier occupies a classical U-shaped valley contributing its meltwater to Morales River, with open crevasses in areas of extending ice flow and two distinctive icefalls located at 3,780–3,750 m asl and 3,160–3,120 m asl in which large seracs contributes to dry-calving.

Yeso and Bello glaciers occupy a southward valley which runs parallel to Pirámide glacier, the largest one which fills out its own catchment. The three large glaciers contribute meltwater to Plomo river. Yeso and Bello are two neighboring clean-ice glaciers located at high-altitude, fully crevassed, with land-terminating tongues and well-defined geometry. At Yeso glacier, the higher icefall is located at an elevation of 4,550–4,500 m asl and a larger one at a lower elevation between 4,440–4,340 m asl. Bello glacier is nourished from three main cirques which form a morphological system of two lateral moraines. The Pirámide glacier is a debris-covered glacier exposed southward with typical hummocky topography composed by furrows and ridges.

**Table 1: Morphometric Characteristics of Five Glaciers Studied in Central Andes**

Glacier Name	Area (km <sup>2</sup> )	Surface	Mean Elevation (m)	UTM Coordinates		Catchment
San Francisco	1.29	Partially Debris-Covered	3,356	400280	6264998	Maipo
Echaurren Norte	0.23	Fully Debris-Covered	3,753	394817	6283501	Maipo
Pirámide	4.40	Debris-Covered	3,664	417141	6284647	Maipo
Yeso	2.03	Clean-Ice	4,420	414293	6289365	Maipo
Bello	4.22	Clean-Ice	4,438	412096	6290018	Maipo

## Data and Methods

### DEM Creation

Airborne LiDAR surveys available were carried out in late-summer season of 2009 for Echaurren Norte and San Francisco glaciers, and in 2012 for Yeso, Bello and Pirámide glaciers; and all the five glaciers were resurveyed in 2015 (Table 2). In April 2015, a total number of 56 GCP were measured along the central flow line (Table 2) on those five mountain glaciers using a geodetic-quality differential GPS (Trimble R6), in a date close to the airborne survey, then it is referred as near-time. GPS used ablation stakes buried on glacier ice at Echaurren Norte, San Francisco, Yeso and Bello glaciers, as well as cruxes on Pirámide glacier (Figure 1), are referred to the World Geodetic System 1984 (WGS84) datum and Universal Transverse Mercator (UTM) projection (zone 19S).

**Table 2: Dates of Specific LiDAR Surveys Available for DEMs Creation and the Ground Control points (GCPs) Measurements in each Glacier to Geo-Reference Ablation Stakes**

Glacier Name	Lidar DEM 0	Lidar DEM 1	GCP measurements
San Francisco	29-04-2009	02-04-2015	20-03-2015
Echaurren Norte	29-04-2009	02-04-2015	15-03-2015
Pirámide	22-04-2012	02-04-2015	14-04-2015
Yeso	22-04-2012	02-04-2015	23-04-2015
Bello	22-04-2012	02-04-2015	22-04-2015

Based upon LiDAR cloud points, a DEM for each glacier was created using the Point Data Abstraction Library (PDAL) software. Interpolation (Z<sub>p</sub>) from different combination of parameters such as spatial resolution (r) and radius of influence (d) in data pre-processing were tested for DEM creation using inverse distance weighted (IDW), triangular irregular network (TIN), natural neighbor (NN) and kriging (KR) algorithms.

The spatial resolution of the pixel (r, ranging from 0,5 to 3,5 m) and the interpolation radius (d, up to 5m), which is the maximum distance of observed points ( $d=r\sqrt{2}$ ), was selected for the best estimates using different combinations, according to the following relation:

$$z_p = \frac{\sum_{i=1}^n \left( \frac{z_i}{d_i^p} \right)}{\sum_{i=1}^n \left( \frac{1}{d_i^p} \right)} \quad (1)$$

Where: z<sub>i</sub> is the value for the point I measured, n is the number of points measured, (p) controls the influence of observed points, and it has a default value of 1.0.

### Accuracy Assessment by using GCP

Once the interpolation algorithm was chosen, then we test the accuracy of the interpolation parameters, aiming to compare biases in the mass balance induced by interpolation parameters only. To do this we changed both spatial resolution (r) and radius of influence (d) in data pre-processing for obtaining the DEM with the minimum RMSE and the DEM with maximum RMSE, hereafter DEM<sub>min</sub> and DEM<sub>max</sub>, respectively, with which both systematic (sys) and random errors (rand) using GCP at glacierized areas ( $\sigma_{GCP,sys}$ ) were derived.

To select the interpolation algorithm which better represents the glacier elevation topography, the RMSE was calculated for all four algorithms using 56 GCPs with their corresponding coordinates in each DEM created. The validation of the DEM with GCP data was used to derive systematic uncertainties (sys) for the DEM/2015 for each glacier, using the following expression [3]:

$$\sigma_{GCP,sys} = \frac{\sum_{i=1}^n h_{DEM} - h_{GCP}}{n} \quad (2)$$

Where  $\sigma_{GCP,sys}$  is the systematic error, n is the number of GCPs, and h is the elevation from DEM and GCPs, respectively. The results for the IDW algorithm are given in Table 3 for the combinations which gave the minimum and maximum RMSE tested with the 56 GCPs.

**Table 3: Elevations derived from global positioning system (GPS) and their corresponding values at pixel size in the digital elevation models (DEMs) with minimum and maximum RMSE using the IDW algorithms which better represents the glacier elevation topography**

Points	Glaciers	East UTM	North UTM	Elevation GPS	Elevation DEM min	Elevation DEM max
1	San Francisco	400395.82	6265803.19	3718.56	3719.43	3719.80
2	San Francisco	400558.55	6265151.14	3418.99	3420.36	3420.22
3	San Francisco	400501.37	6265191.03	3433.47	3434.51	3434.76
4	San Francisco	400623.54	6264992.68	3385.95	3387.02	3387.00
5	San Francisco	400477.56	6265016.55	3377.91	3379.18	3378.96
6	San Francisco	400197.53	6264750.91	3272.34	3272.35	3273.57
7	San Francisco	400192.96	6264758.2	3274.59	3275.81	3275.94
8	San Francisco	400065.88	6264405.04	3193.71	3194.54	3194.24
9	San Francisco	400060.98	6264429.66	3200.00	3200.67	3201.02
10	San Francisco	399977.66	6264137.25	3021.07	3022.34	3022.14
11	San Francisco	399976.74	6264094.99	3006.52	3007.63	3007.41
12	San Francisco	399998.95	6263889.15	2922.26	2923.51	2924.30
13	San Francisco	400088.45	6263636.79	2839.91	2840.58	2841.44
14	San Francisco	400091.92	6263642.63	2841.60	2842.78	2842.84
15	San Francisco	400096.55	6263638.14	2837.73	2837.83	2838.96
16	San Francisco	400356.71	6263375.73	2705.02	2705.08	2705.81
17	San Francisco	400353.66	6263384.9	2706.56	2706.57	2707.21
18	Echaurren Norte	395157.45	6284245.31	3844.04	3844.92	3844.89
19	Echaurren Norte	394901.48	6284169.67	3799.62	3800.58	3800.77
20	Echaurren Norte	394989.07	6284117.97	3780.97	3781.59	3781.83
21	Echaurren Norte	394905.55	6284026.4	3760.77	3761.39	3761.85
22	Echaurren Norte	394726.17	6283839.55	3750.05	3750.90	3751.54
23	Echaurren Norte	394784.02	6283803.81	3726.31	3726.76	3727.20
24	Echaurren Norte	394814.18	6283759.87	3713.17	3714.30	3714.65
25	Echaurren Norte	394721.00	6283619.47	3693.74	3694.83	3694.86
26	Echaurren Norte	394657.14	6283656.15	3711.62	3712.95	3712.90
27	Echaurren Norte	394568.14	6283700.34	3757.46	3757.90	3758.74
28	Echaurren Norte	394504.81	6283612.3	3750.85	3751.77	3751.76
29	Echaurren Norte	394619.93	6283560.91	3709.68	3710.72	3710.73
30	Echaurren Norte	394688.03	6283487.19	3684.82	3685.82	3685.90
31	Pirámide	416779.71	6286735.43	3869.11	3868.35	3868.17
32	Pirámide	416886.06	6286251.12	3818.16	3817.95	3817.36
33	Pirámide	417079.86	6285595.18	3740.68	3740.58	3740.65
34	Pirámide	417257.58	6284911.04	3679.85	3679.63	3679.58
35	Pirámide	417311.34	6284388.64	3630.19	3629.85	3629.95
36	Pirámide	417356.32	6284021.02	3583.62	3583.57	3583.52
37	Pirámide	417491.40	6283674.25	3540.77	3540.92	3540.97
38	Pirámide	417511.46	6282800.77	3448.32	3447.89	3446.67
39	Pirámide	417326.77	6282092.38	3392.09	3391.86	3392.41
40	Pirámide	417036.09	6281610.75	3369.99	3369.62	3368.74
41	Yeso	414262.45	6289925.33	4570.55	4570.80	4570.79
42	Yeso	414563.82	6289792.37	4492.27	4492.89	4492.71
43	Yeso	414584.60	6288768.45	4302.03	4303.11	4302.23
44	Yeso	414106.86	6288252.14	4121.88	4123.15	4122.01
45	Bello	411188.01	6290342.21	4535.06	4535.47	4535.34

46	Bello	411713.88	6289724.61	4364.79	4365.88	4366.17
47	Bello	411707.49	6289841.1	4367.78	4368.46	4368.45
48	Bello	412012.30	6289874	4362.71	4363.10	4363.30
49	Bello	412010.45	6289889.81	4364.97	4365.35	4365.65
50	Bello	412543.48	6289193.56	4196.19	4196.71	4196.67
51	Bello	413010.79	6288715.52	4081.91	4082.49	4081.89
52	Bello	412030.83	6290453.59	4435.44	4435.97	4436.38
53	Bello	411957.90	6290374.49	4419.68	4420.29	4420.10
54	Bello	412338.34	6290428.41	4479.76	4480.14	4480.71
55	Bello	411737.57	6290261.2	4423.74	4424.34	4424.46
56	Bello	412366.09	6289937.25	4390	4390.46	4390.66

### Accuracy Assessment by using Rocky Areas

The control area (AC) on unchanged non-glacierized rocky areas between surveys was determined considering flat slopes surfaces (<35°) for avoiding steep areas. This procedure avoids elevation differences induced by landslides from stepped and recently deglaciated unstable slopes as well as variations associated with changes in isolated ice masses.

To derive elevation bias of both DEMmin and DEMmax, overlaid pixels on stable rocky terrain outside the glacier outlines, covering 52.6 ha in total, were used to retrieve the systematic uncertainty ( $\sigma_{sys}$ ) in the control area ( $\sigma_{AC,sys}$ ) (Table 3).

$$\sigma_{AC,sys} = \frac{\sum_1^n h_{DEMmin} - h_{DEMmax}}{n} \quad (3)$$

The resulting uncertainties are given in Table 4 for the combinations giving the minimum and maximum RMSE tested with the GCP.

**Table 4: Glacier surface elevation change (dh/dt) and accuracy assessment using ground control point (GCP), rocky control areas and random uncertainty, according to interpolation parameters per glacier**

Glacier Name	Interpolation parameters		$\overline{\frac{\partial h}{\partial t}}$ (m)	Accuracy using GPC				Accuracy using rocky control area				Random uncertainty		
	r (m)	d (m)		RMSE	$\sigma_{GCP,sys}$ (m)	$\sigma_{\frac{\partial v}{\partial t}}$	$\sigma_M$ (Kton)	Control Area (km <sup>2</sup> )	$\sigma_{CA,sys}$ (m)	$\sigma_{\frac{\partial v}{\partial t}}$	$\sigma_M$ (Kton)	$\overline{\frac{\partial h}{\partial t}}$ (m)	$\sigma_{\frac{\partial v}{\partial t}}$ (m <sup>3</sup> )	$\sigma_M$ (Kton)
San Francisco	3.5	4.959	-11.40	1.19	0.86	1,454,905	1,237	0.181	0.62	1,048,885	892	0.018	30,886	1,158
	0.75	1.061	-11.77	0.95	0.57	959,261	815		0.81	1,363,160	1,159	0.007	11,784	1,189
Echaurren Norte	2	3.536	-9.06	0.91	0.87	200,302	170	0.191	0.03	6,907	6	0.023	5,227	125
	0.5	0.707	-9.08	1.14	1.12	257,180	219		0.08	18,370	16	0.006	1,321	125
Pirámide	3.5	4.95	-0.68	0.78	0.47	1,647,601	1,400	0.080	1.18	4,136,530	3,516	0.007	23,326	143
	0.75	1.414	-0.79	0.35	0.25	873,315	742		0.95	3,318,599	2,820	0.001	4,821	168
Yeso	3.5	4.95	-1.97	0.90	0.25	431,209	367	0.038	0.52	896,915	762	0.009	15,808	204
	0.5	0.707	-2.24	0.27	0.80	1,379,642	1,173		0.40	689,821	586	0.001	2,337	232
Bello	2.5	3.536	-2.23	0.72	0.64	2,304,088	1,958	0.036	1.21	4,356,166	370	0.004	14,218	482
	0.75	4.95	-2.29	0.58	0.55	1,966,928	1,672		0.78	2,789,462	2,371	0.001	4,093	493

### Random Uncertainty of the DEM

Random or stochastic uncertainties for geodetic mass balances regard to three main sources of independent uncertainties from: (i) the standard deviation ( $\sigma_z$ ) in the surface elevation change (dh/dt) (ii) glacier area delimitation ( $\sigma_A$ ) corrected from drawing buffers around the glacier outline, and (iii) density conversion factor from volume to mass ( $\sigma_\rho$ ). Then we calculated the random uncertainty for elevation ( $\sigma_{\frac{\partial h}{\partial t}}$ ), volume ( $\sigma_{\frac{\partial v}{\partial t}}$ ) and mass ( $\sigma_M$ ) using both GCP and rocky areas for further calculation on geodetic mass balances and glaciological interpretation [21,22].

We use a value given in literature for glacier ice of 850 kg m<sup>-3</sup> for the ice-density conversion factor with an uncertainty of 60 kg m<sup>-3</sup> [32]. The expression to obtain the random error for the elevation, volume and mass difference are the following:

$$\sigma_{\frac{\partial h}{\partial t}} = \frac{SD}{\sqrt{n}} \quad (4)$$

$$\sigma_{\frac{\partial V}{\partial t}} = \sqrt{\left(\sigma_A \cdot \frac{\partial V}{\partial t}\right)^2 + \left(\sigma_{\frac{\partial h}{\partial t}} \cdot A\right)^2} \quad (5)$$

$$\sigma_M = \sqrt{\left(\sigma_{\frac{\partial V}{\partial t}} \cdot f_\rho\right)^2 + \left(\sigma_{f_\rho} \cdot \frac{\partial V}{\partial t}\right)^2} \quad (6)$$

Where SD is the standard deviation for the elevation difference of the DEMs and n is the number of grids [3]. The results for each one of the values in the expressions and the results are given in Table 4 for the combinations that gave the minimum and maximum RMSE tested with the GCP.

### Total Uncertainty of the DEM

Total error of the DEM has been calculated considering both random (rand) and systematic (sys) errors for elevation ( $\sigma_h$ ), volume ( $\sigma_v$ ), mass balance ( $\sigma_M$ ) and its water equivalent ( $\sigma_B$ ), with the following expression given by Pelto [23]. The results are shown in Table 4

$$\sigma_h = \sqrt{(\sigma \Delta h_{rand})^2 + (\sigma \Delta h_{sys})^2} \quad (7)$$

$$\sigma_v = \sqrt{(\sigma \Delta V_{rand})^2 + (\sigma \Delta V_{sys})^2} \quad (8)$$

$$\sigma_M = \sqrt{(\sigma \Delta M_{rand})^2 + (\sigma \Delta M_{sys})^2} \quad (9)$$

$$\sigma_B = \sqrt{(\sigma \Delta B_{rand})^2 + (\sigma \Delta B_{sys})^2} \quad (10)$$

### Geodetic Mass Balance

We determined the volume change ( $\Delta V$ ), which is the mass balance of the glacier, in cubic meters by subtracting elevation values at pixel scale in overlaid areas between two DEMs, using the union module in the open-source Quantum Geographic Information System software (QGIS) with the following expression:

$$\Delta V = r^2 \cdot \sum_{k=1}^K \Delta h_k \quad (m^3) \quad (11)$$

Where k is the number of pixels covering the glacier area;  $\Delta h_k$  is the elevation difference between two areas in the pixel k, and r is the resolution of the pixel.

The volume change was then converted to mass change ( $\Delta M$ ) using the conversion factor of  $850 \pm 60$  ( $\text{kgm}^{-3}$ ) recommended by Huss if the data accomplish the following criteria: (i) the study period is greater than 3 years, (ii) volume changes observed (iii) there are no strong changes in the mass balance gradient. How it approves the criteria, the following expression is used to determine the mass difference [32]:

$$\Delta M = (f_{\Delta V} \pm \sigma_{dc}) \cdot \Delta V \quad (kg) \quad (12)$$

Finally, the geodetic mass balance ( $B_{geod}$ ) was determined as the difference in mass divided by water density ( $\rho=1000$  ( $\text{kg}\cdot\text{m}^{-3}$ ) and the glacier area according to the following expression.

$$B_{geod} = \frac{\Delta M}{1000 \cdot S_m} \quad (m) \quad (13)$$

The resulting surface elevation change ( $dh/dt$ ) becomes the inter-annual rate dividing it by the spanning time ( $\text{m a}^{-1}$ ), in which elevation bias is estimated using both GCP and rocky areas, together with their random uncertainty (Table 5).

**Table 5: Geodetic mass balances and their corresponding errors using ground control points (GCP) and rocky control areas, according to interpolation parameters per glacier**

Glacier Name	Interpolation Parameters		Geodetic Mass Balance with Total Error using GCP		Geodetic Mass Balance with Total Error using Rocky Control Area	
	r (m)	d (m)	$\Delta B_{geo} \pm \sigma_{B_{geo}}$ (m)	$\Delta B_{geo} \pm \sigma_{B_{geo}}$ (m eq. w. yr <sup>-1</sup> )	$\Delta B_{geo} \pm \sigma_{B_{geo}}$ (m)	$\Delta B_{geo} \pm \sigma_{B_{geo}}$ (m eq. w. yr <sup>-1</sup> )
San Francisco	3.5	4.959	$-9.69 \pm 1.00$	$-0.751.64 \pm 0.17$	$-9.69 \pm 0.86$	$-1.64 \pm 0.15$
	0.75	1.061	$-10.01 \pm 0.86$	$-1.69 \pm 0.14$	$-10.01 \pm 0.99$	$-1.69 \pm 0.17$
Echaurren Norte	2	3.536	$-7.68 \pm 0.92$	$-1.30 \pm 0.15$	$-7.68 \pm 0.54$	$-1.30 \pm 0.09$
	0.5	0.707	$-7.72 \pm 1.10$	$-1.30 \pm 0.19$	$-7.72 \pm 0.55$	$-1.30 \pm 0.09$
Pirámide	3,5	4.95	$-0.57 \pm 0.40$	$-0.19 \pm 0.14$	$-0.57 \pm 1.00$	$-0.19 \pm 0.34$
	0.75	1.414	$-0.68 \pm 0.22$	$-0.23 \pm 0.07$	$-0.68 \pm 0.81$	$-0.23 \pm 0.27$
Yeso	3.5	4.95	$-1.67 \pm 0.24$	$-0.57 \pm 0.08$	$-1.67 \pm 0.46$	$-0.57 \pm 0.16$
	0.5	0.707	$-1.90 \pm 0.69$	$-0.65 \pm 0.24$	$-1.90 \pm 0.37$	$-0.65 \pm 0.12$
Bello	2.5	3.536	$-1.90 \pm 0.56$	$-0.64 \pm 0.19$	$-1.90 \pm 1.04$	$-0.64 \pm 0.35$
	0.75	4.95	$-1.95 \pm 0.49$	$-0.66 \pm 0.17$	$-1.95 \pm 0.68$	$-0.66 \pm 0.23$

## Results and Discussion

### Interpolation Parameters

Ground-truth validation of inverse distance weighted (IDW), triangular irregular network (TIN), natural neighbor (NN) and kriging (KR) algorithms for DEM creation are shown in Table 6. All the interpolation parameters combining both spatial resolution (r) and radius of influence (d) in data pre-processing tested yields sub metric RMSEs. However, the most accurate result was obtained when using the IDW algorithm, an achievement which confirms the efficiency of the IDW algorithm in DEM creation for glaciological applications [33]. The minimum and maximum RMSE obtained for each GPC after testing different combinations using the IDW, are shown in Table 6. In spite that all the other combinations resulted in sub-metric RMSE, elevation values interpolated are positives and

negatives regarding to GCPs and random spatial differences on glacier surface are due to changes in the interpolation parameters only.

**Table 6: Root-mean square error (RMSE) according to spatial resolution and mean RMSE obtained after comparing 56 GCP surveyed with global positioning system (GPS) with the DEM created the inverse distance weighted (IDW), triangular irregular network (TIN), natural neighbor (NN) and kriging (KR) algorithms for DEM creation. Although all the algorithms yielded sub-metric errors, the IDW algorithm represents the glacier elevation topography accurately**

Spatial Resolution (m)	IDW	NN	TIN	KG
0.5	0.944	0.943	0.949	0.952
0.75	0.911	0.911	0.955	0.948
1.00	0.9	0.94	0.970	0.976
1.5	0.878	0.867	0.938	0.951
2.00	0.806	0.931	0.968	0.970
Mean	0.887	0.918	0.956	0.959

The minimum RMSE of 0.272 was found at Yeso glacier and the maximum RMSE of 1.189 at San Francisco glacier. It can be noticed that although the spatial resolution varies between 0.5 and 3.5 m of pixel sizes, the related RMSE does not change so much and only in two cases the minimum pixel size obtained, of 0.75 m and 0.5 m, provided the larger RMSE of 1.189 m and 1.135 m, respectively.

The minimum RMSE was obtained using the highest spatial resolution of 0.5 only at Yeso glacier whereas a larger value of 0.75 m was obtained at San Francisco, Pirámide and Bello glaciers, and a maximum of 2 m was obtained for Echaurren Norte glacier.

In the case of San Francisco glacier, the geodetic mass balance yields a difference of 0.32 m, with a larger estimate obtained with the largest spatial resolution of 3.5 m; however, its RMSE is sub-metric. In the case of Echaurren Norte glacier, these differences can be neglected, although the sub-metric RMSE yielded a smaller mass balance estimate.

Differences in geodetic mass balance, by changing the interpolation parameters, is 0.23 m for Yeso glacier, with a larger estimate when using the maximum resolution of 0.5 m, and the DEM with the minimum RMSE. At Bello glacier, the relation between minimum RMSE and larger mass balance estimates becomes inverse, spatial resolution of 0.75 and 2.5 m did not show any significant bias. At Pirámide glacier, the high spatial resolution of 0.75 m yields a larger mass balance estimate of 0.04 m, w.e. a<sup>-1</sup>, which is consistent after validation of GCP.

#### Accuracy Assessment using GCP

Vertical accuracy of both high-resolution DEMs compared with its corresponding GCP values at pixel size is presented at Table 3. It can be firstly noticed that the mean differences between airborne data and GCP is ±0.58 and ±0.67 m, respectively, which is larger than the expected vertical accuracy of ±0.3 m after post-processing in LiDAR surveys [17]. Secondly, jagged topography such as highly crevassed and penitent areas in case of clean-ice glaciers as well as boulders and thermokarst in debris-covered glaciers, contain height differences of up to 2m within a square meter on glacier surface which hampers the interpolation of a single elevation value for the algorithms when DEM is created (Figure 2).



**Figure 2:** Glacier surface conditions on Bello glacier in November 2021. Note the existence of ice pinnacles of up to 2 m which hampers the definition of an elevation value at pixel size. The ice axe height is 66 cm

Surface elevation change at San Francisco and Echaurren Norte glaciers obtained using both RMSE, is 0.32 m and 0.02 m, which is less than the systematic error obtained using the GCP of 0.57 and 0.86 m, respectively (Table 4). The systematic error is consistent with the RMSE previously derived, and its larger value at both the glaciers is found with the smallest pixel value for interpolation. This difference is also found at Pirámide, Yeso and Bello glaciers in which the difference between the DEMs is smaller than the error associated (Table 4).

In the case of San Francisco glacier, the minimum systematic error of 0.62 m was obtained using the finer spatial resolution of 0.75 m whereas its coarser resolution of 3.5 m only increases the error up to 0.81 using a sub-metric RMSE with a radius of influence of 4.96 m. When using high-resolution data this error becomes smaller than 0.86 but still larger than the GCP at 3.5 m resolution. At Echaurren Norte glacier both systematic errors can be neglected, and they are two orders of magnitude smaller than those derived with GCP.

#### Accuracy Assessment using Rocky Areas

The results for the surface elevation change, volume, mass, and geodetic mass balance are given in Table 5 for the combinations resulted from the minimum and maximum RMSE tested with both the GCP and rocky areas, respectively.

The largest negative mass balance was achieved at San Francisco glacier, a thinning rate which is larger than the worldwide trend of -0.54 m w.e. a<sup>-1</sup> estimated for the second half of the 20th century whereas the minimum rate was achieved at Pirámide debris-covered glacier [2]. In this latter and unique case, the accuracy assessment becomes important since the thinning rate can be misrepresented when the estimated error using rocky areas is larger than the magnitude of change.

The spatial distribution of thinning rates of the five glaciers studied is presented in Figure 3. Because all the glaciers share the same climate, the mean elevation is suitable to explain the largest thinning rates derived at San Francisco and Echaurren Norte glaciers whereas more moderate rates are found at Bello and Yeso glaciers, located at a higher altitude.

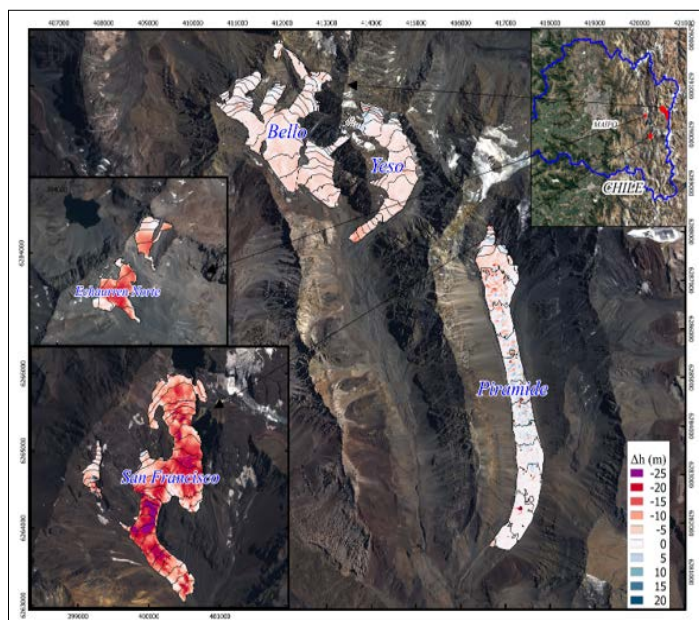


**Figure 3:** Geodetic mass balances per year in water equivalent ( $m\ w.e.\ a^{-1}$ ) from surface elevation change ( $dh/dt$ ) derived by repeated LiDAR surveys per glacier. The highest thinning rate is found at San Francisco and Echaurren Norte glaciers in which it extends mostly to the entire glacier area, located at lower elevations ( $<4,000\ m\ asl$ ). More moderate thinning rates are found at high-altitude Bello and Yeso glaciers, with maximum values at lower elevations but still showing evidence of thinning over  $>4,500\ m\ asl$ . At Pirámide glacier the thinning rate is the smallest one.

The entire glacier area of San Francisco and Echaurren Norte glaciers are exposed to thinning conditions and the bare ice predominates on glacier surface at the end of summer. Glaciers are getting fully covered of debris as glacier down wasting increases at lower elevations ( $<4,000\ m\ asl$ ) and surrounding steeped slopes become unstable. At Bello and Yeso glaciers the ice thinning is also affecting lower areas although thinning over  $>4,500\ m\ asl$  is more moderate but still affecting at high-altitude. The smallest thinning rate estimated at Pirámide glacier is largely explained by the insulated effect of debris which protect the underlying ice from ablation.

Geodetic mass balance profiles according to the distribution of areas by elevation at  $50\ m$  bins is presented in Figure 4. The profiles show both substantial and generalized ice thinning at low elevations ( $<4,000\ m\ asl$ ) and decreasing it towards higher elevation. Positive thickening values at Yeso and Pirámide glaciers are due to compressive flow at specific sites but irrelevant for long-term thinning rate.

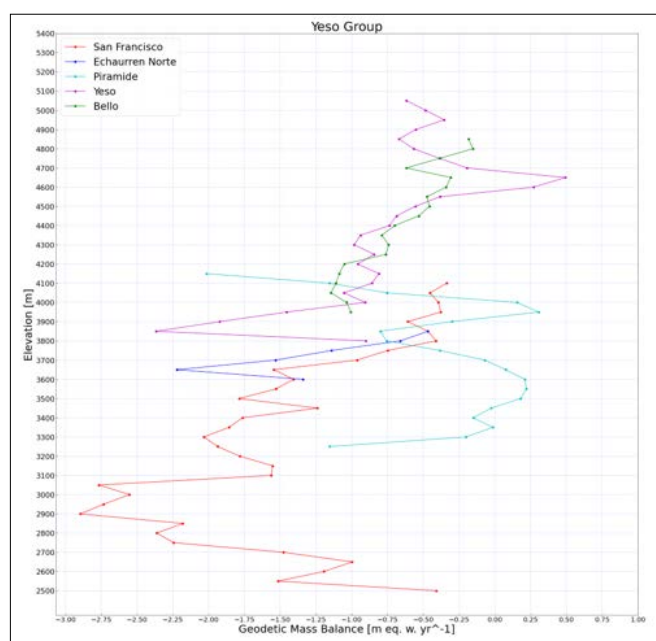


**Figure 4:** Geodetic mass balance profiles according to the distribution of areas by elevation at  $100\ m$  bins. Zigzag patterns with the elevation are due to local factors such as aspect, debris-coverage (thin/thick) and exposure to solar radiation accounting for glacier response. The profiles show both substantial and diverse thinning at low elevations ( $<4,000\ m\ asl$ ) demonstrating that glaciers react to global warming in a complex way. Positive thickening values at Yeso and Pirámide glaciers are due to compressive flow.

The oscillating zigzag patterns strongly suggest the influence of natural factors at local scales such as heat exchange, radiation and turbulent fluxes affecting the surface energy-balance, which demonstrates the fact that glaciers react to global warming in a complex way. The lengthening of the ablation season in addition to aspect, debris-coverage (thin/thick) and exposure to solar radiation are important accounting for glacier response.

### Conclusion

Airborne light radio detection and ranging (LiDAR) altimetry data for geodetic mass balances in Central Andes and its near-time ground-truth data was first used for validation. Vertical accuracy of DEMmin from LiDAR data is  $\pm 0.58$  m, a larger value than expected one to use IMU only, which accounts as systematic errors for total uncertainty of the DEM. High thinning rates of up to  $-1.69 \pm 0.14$  m at case San Francisco Glacier far exceed worldwide trend which is a clear indicator that global warming hits the entire glacier areas during an extended ablation season.

In the absence of ground-truth data, accuracy assessment using non-glacierized rocky areas provides negligible differences regarding to GCP on glacier surface, and the main source of uncertainty comes from pre-processing of interpolation parameters. The IDW algorithm reproduced the topography accurately, and the interpolation parameters in DEM creation should be decided according to ground reconnaissance. Since sub metric pixel size sometime yields inaccurate outputs in DEM creation, biases in geodetic mass balances induced by interpolation parameters yield differences of up to 3%, a bias which lies within the systematic errors derived using GCPs.

A sub-metric RMSE is suitable for accurate results when the magnitude of elevation change is large enough than error estimates as the case of Echaurren Norte and San Francisco glacier, with repeat LiDAR surveys spanning for more than 5 years interval. However, other error sources such as glacier outlines and ice-density also account for the total accuracy of the DEM. In spite the use of high-resolution data ( $< 3.5$  m) appears to provide more accurate outcomes, ground-truth validation indicates that other factors such as glacier surface roughness are relevant parameters to obtain a representative elevation value at pixel size. In glaciers with gentle topography a high spatial resolution (0.5 m) is preferable; on the other hand, a coarser spatial resolution (3.5 m) is suitable for jagged glaciers to avoid the influence of highly crevassed areas, rock boulders and ice penitents ( $> 1$  m height within  $1\text{m}^2$ ) on glacier surface [34,35].

### Author Contribution Statement

GB established the research problem and wrote the manuscript. FG, processed the data sets, prepared the figures, tables, and contributed to the manuscript. All other authors, XF, GP, FMc and FC-B contributed to scientific discussion and improvement of the scientific achievement of the manuscript. The contribution of Alekos Sanllehi and Karina Vallejos in data analysis is greatly appreciated.

### Conflict of Interest

The authors declare no conflict of interest.

### Acknowledgement

The authors thank the National Research and Development Agency (ANID) from the Ministerio de Ciencia, Tecnología, Conocimiento e Innovación of Chile for financial support of projects ANID-ANILLO ACT210021, ANID-FONDECYT REGULAR 1221526

and FOVI 230167. Dirección General de Aguas (DGA) provided both LiDAR data available and ground-truth surveys in 2015. Ground surveys were carried out by GB together with Raúl Cisternas, Jorge Huenante, Carlos Mendoza, Diego González and Antonio Vergara, all of them at DGA in 2015. The technical skill of Terra Remote Sensing Ltda and Digimapas Ltda, both Consulting Companies, is greatly appreciated. Special thanks to Dr. Markus Rombach and Mr. Fulvio Cortés.

### References

1. Gardner A, Moholdt G, Cogley G, Wouters B, Arendt A, et al. (2013) A Reconciled Estimate of Glacier Contributions to Sea Level Rise: 2003 to 2009. *Science* 340: 852-857.
2. Zemp M, Frey H, Gärtner Roer I, Nussbaumer S, Hoelzle M, et al. (2015) Historically unprecedented global glacier decline in the early 21st century. *Journal of Glaciology* 61: 745-762.
3. Koblet T, Gärtner Roer I, Zemp M, Jansson P, Thee P, et al. (2010) Reanalysis of multi-temporal aerial images of Storglaciären, Sweden (1959–99)–Part 1: Determination of length, area, and volume changes. *The Cryosphere* 4: 333-343.
4. Paul F, Kääb A, Maisch M, Kellenberger T, Haerberli W (2004) Rapid disintegration of Alpine glaciers observed with satellite data. *Geophysical Research Letters* 31: 21402.
5. Ming J, Wang Y, Du Z, Zhang T, Guo W, et al. (2015) Widespread albedo decreasing and induced melting of Himalayan Snow and Ice in the Early 21st Century. *Plos One* 10: 0126235.
6. Cereceda Balic F, Ruggeri MF, Vidal V, Ruiz L, Fu J (2022) Understanding the role of anthropogenic emissions in glaciers retreat in the central Andes of Chile. *Environmental Research* 214: 113756.
7. Hagen J, Reeh N, Bamber J, Payne A (2004) In situ measurement techniques: Land ice. In J. Houghton (Author) & (Eds.), *Mass Balance of the Cryosphere: Observations and Modelling of Contemporary and Future Changes*. Cambridge: Cambridge University Press 11-42.
8. Cuffey KM, Paterson WSB (2006) *The physics of glaciers*. Academic Press. <https://shop.elsevier.com/books/the-physics-of-glaciers/cuffey/978-0-12-369461-4>.
9. Østrem G, Brugman M (1991) *Glacier massbalance measurements: a manual for field and office work*, Saskatoon: National Hydrology Research Institute, and Oslo. The Norwegian Water Resources and Electricity Board. [https://wgms.ch/downloads/Oestrem\\_Brugman\\_GlacierMassBalanceMeasurements\\_1991.pdf](https://wgms.ch/downloads/Oestrem_Brugman_GlacierMassBalanceMeasurements_1991.pdf).
10. Cogley JG (2009) Geodetic and direct mass-balance measurements: comparison and joint analysis. *Annals of Glaciology* 50: 096-100.
11. Lee I, Chang HC, Ge L (2005) GPS campaigns for validation of InSAR derived DEMs. *Journal of Global Positioning Systems* 4: 82-87.
12. Cox LH, March RS (2004) Comparison of geodetic and glaciological mass-balance techniques, Gulkana Glacier, Alaska, USA. *Journal of Glaciology* 50: 363-370.
13. König M, Winther J, Isaksson E (2001) Measuring snow and glacier ice properties from satellite. *Reviews of Geophysics* 39: 01-27.
14. Barcaza G, Aniya M (2007) Application of remote sensing to glacier studies. *Seppyo* 69: 201-220.
15. Zemp M, Thibert E, Huss M, Stumm D, Rolstad Denby C, et al. (2013) Reanalysing glacier mass balance measurement series. *The Cryosphere* 7: 1227-1245.
16. Shean DE, Alexandrov O, Moratto ZM, Smith BE, Joughin IR, et al. (2016) An automated, open-source pipeline for

- mass production of digital elevation models (DEMs) from very-high-resolution commercial stereo satellite imagery. *ISPRS Journal of Photogrammetry and Remote Sensing* 116: 101-117.
17. Hodgson ME, Bresnahan P (2004) Accuracy of airborne lidar-derived elevation. *Photogrammetric Engineering & Remote Sensing* 70: 331-339.
  18. Belart J, Magnússon E, Berthier E, Gunnlaugsson ÁÞ, Pálsson F, et al. (2020) Mass balance of 14 Icelandic glaciers, 1945–2017: spatial variations and links with climate. *Frontiers in Earth Science* 8: 163.
  19. Favey E, Wehr A, Geiger A, Kahle HG (2002) Some examples of European activities in airborne laser techniques and an application in glaciology. *J Geodyn* 34: 347-355.
  20. Baltsavias EP, Favey E, Bauder A, Bosch H, Pateraki M (2001) Digital surface modelling by airborne laser scanning and digital photogrammetry for glacier monitoring. *The Photogrammetric Record* 17: 243-273.
  21. Rolstad C, Haug T, Denby B (2009) Spatially integrated geodetic glacier mass balance and its uncertainty based on geostatistical analysis: Application to the western Svartisen ice cap, Norway. *Journal of Glaciology* 55: 666-680.
  22. Granshaw FD, Fountain AG (2006) Glacier change (1958–1998) in the north cascades national park complex, Washington, USA. *J Glaciol* 52: 251-256.
  23. Pelto BM, Menounos B, Marshall SJ (2019) Multi-year evaluation of airborne geodetic surveys to estimate seasonal mass balance, Columbia and Rocky Mountains, Canada. *The Cryosphere* 13: 1709-1727.
  24. Basantes Serrano R, Rabatel A, Vincent C, Sirguey P (2018) An optimized method to calculate the geodetic mass balance of mountain glaciers. *Journal of Glaciology* 64: 917-931.
  25. Barcaza G, Nussbaumer SU, Tapia G, Valdés J, García JL, et al. (2017) Glacier inventory and recent glacier variations in the Andes of Chile, South America. *Annals of Glaciology* 58: 166-180.
  26. Masiokas M, Christie D, Le Quesne C, Pitte P, Ruiz L, et al, (2016) Reconstructing the annual mass balance of the Echaurren Norte glacier (Central Andes, 33.5°S) using local and regional hydroclimatic data. *Cryosphere* 10: 927-940.
  27. Masiokas MH, Rabatel A, Rivera A, Ruiz L, Pitte P, et al. (2020) A review of the current state and recent changes of the Andean cryosphere. *Frontiers in Earth Science* 8: 99.
  28. Falvey M, Garreaud RD (2009) Regional cooling in a warming world: Recent temperature trends in the southeast Pacific and along the west coast of subtropical South America (1979–2006). *Journal of Geophysical Research* 114: 04102.
  29. Boisier JP, Rondanelli R, Garreaud RD, Muñoz F (2016) Anthropogenic and natural contributions to the Southeast Pacific precipitation decline and recent megadrought in central Chile. *Geophysical Research Letters* 43: 413-421.
  30. Garreaud R, Boisier JP, Rondanelli R, Montecinos A, Sepúlveda H, et al. (2019) The central mega drought (2010-2018): a climate dynamics perspective. *Int J Climatol* 01-19.
  31. Nuth C, Kohler J, Aas HF, Brandt O, Hagen JO (2007) Glacier geometry and elevation changes on Svalbard (1936–90): a baseline dataset. *Ann Glaciol* 46: 106-116.
  32. Huss M (2013) Density assumptions for converting geodetic glacier volume change to mass change. *The Cryosphere* 7: 877-887.
  33. Ashraf I, Hur S, Park Y (2017) An investigation of interpolation techniques to generate 2D intensity image from LIDAR data. *IEEE Access* 5: 8250-8260.
  34. Aldunce P, Araya D, Sapiain R, Ramos I, Lillo G, et al. (2017) Local perception of drought impacts in a changing climate: The mega-drought in central Chile. *Sustainability* 9: 2053.
  35. Haug T, Rolstad C, Elvehøy H, Jackson M, Maalen Johansen I (2009) Geodetic mass balance of the western Svartisen ice cap, Norway, in the periods 1968–1985 and 1985–2002. *Ann Glaciol* 50: 119-125.

**Copyright:** ©2025 Gonzalo Barcaza, et al. This is an open-access article distributed under the terms of the Creative Commons Attribution License, which permits unrestricted use, distribution, and reproduction in any medium, provided the original author and source are credited.